CONF-970231--32 SAN096-2214C

Microstructure and interface properties of laterally oxidized $Al_xGa_{1-x}As$

R.D. Twesten, D.M. Follstaedt, and K.D. Choquette
Sandia National Laboratories, Albuquerque, NM 87185-1056

ABSTRACT

The microstructure and interface properties of $Al_xGa_{1-x}As$ materials that have been laterally oxidized in wet N_2 for several compositions (x=0.80, 0.82 ... 1.00) and temperatures (360°C to 450°C) have been studied. The microstructure is found to be relatively insensitive to composition and oxidation temperature. The oxidation forms an amorphous solid solution $(Al_xGa_{1-x})_2O_3$ that transforms to polycrystalline, γ-$(Al_xGa_{1-x})_2O_3$ under electron beam exposure in the electron microscope. Evidence suggests a small fraction of crystalline $(Al_xGa_{1-x})_2O_3$ is formed via post oxidation annealing of the oxide. The level of hydrogen present in the oxidized layers is $1.1x10^{21}cm^{-3}$, which is too low for the amorphous phase observed to be a hydroxide rather than an oxide. The amount of As in the layer is reduced to < 2atm%, and no As precipitates are observed. The $(Al_xGa_{1-x})_2O_3$ / GaAs interface is abrupt, but prolonged oxidation will cause the GaAs to oxidize at the internal interfaces. The reaction front between the oxidized and the unoxidized $Al_xGa_{1-x}As$ has a 10 to 20nm-wide amorphous zone that shows a different contrast than the remainder of the amorphous oxide and is stable under electron irradiation.

Keywords: vertical-cavity laser, VCSEL, lateral oxidation, AlGaAs, microstructure

1. INTRODUCTION

The selective and passivating nature of the oxidation of high Al content AlGaAs[1] has been used to create high-performance vertical-cavity surface emitting lasers (VCSELs)[2,3,4]. This is accomplished by using the fact the Ga content of a AlGaAs film will drastically affect its oxidation rate[5], allowing the strategic placement of high Al content layers in the structure; these are then oxidized to form current-confining and optical-mode-defining apertures.

In this paper, we discuss the microstructure of the oxide phase formed from the wet oxidation of $Al_xGa_{1-x}As$ with x=0.98,0.92 in actual working VCSEL device structures and for x=0.80, 0.82 ... 1.00 in layered test structures. The oxidation was performed at various temperatures. It is found that the oxide phase formed is amorphous (Al_xGa_{1-x}) oxide, presumably $(Al_xGa_{1-x})_2O_3$ since nonstoichiometric alumina is uncommon[6]. This phase is unstable, transforming to fine grained (~4nm) γ-$(Al_xGa_{1-x})_2O_3$ under electron beam exposure in the transmission electron microscope (TEM). It is also found that the lateral oxidation front terminates with an 10-20nm amorphous zone that is stable under the electron beam. Lattice images show that the oxide terminus makes an abrupt transition from crystalline to amorphous, and lower magnification, strain-contrast images reveal no defects associated with the oxidation front. The interface with the surrounding GaAs is abrupt, but prolonged exposure to the oxidizing environment allows the GaAs to oxidize at the internal interfaces. Also, voids can be formed at the oxide/GaAs interface during electron-beam exposure.

The fate of the As in the oxidized layers is not as clear. Recent reports[7,8] indicate the As is retained in the oxidized layers as elemental As or As_2O_3. Our chemical analysis indicates very little As is retained in the layers, and we have seen no evidence for elemental As precipitates. This discrepancy is currently under investigation but may be due to the significant H content ($1.1x10^{21}cm^{-3}$) of these layers, which has been shown to cause reduction of As_2O_3 to more volatile As and AsH_3 in the oxidized layers[7].

This paper is organized as follows: We first present the experimental methods used to grow, oxidize and characterize these materials. We next report on the oxide phase and chemical composition that results from wet oxidation of $Al_xGa_{1-x}As$. Finally, we describe the structure of the interfaces of the oxide with the surrounding crystal.

2. EXPERIMENTAL

AlGaAs layers were grown using MOVPE on GaAs(001) substrates, which has been reported in detail elsewhere[5]. Three sets of sample material were used in this study: actual working 980nm VCSEL devices and two sets of test structures. The VCSEL devices utilize DBR mirrors which consist of $GaAs/Al_{0.92}Ga_{0.08}As$ layers with para-

DISCLAIMER

bolic composition grading between layers. Two 84-nm layers (one above and one below the active region) of $Al_{0.98}Ga_{0.02}As$ were grown to form a current constricting aperture by subsequent selective oxidation. Trenches were etched to expose the $Al_{0.98}Ga_{0.02}As$ layers at the sides of 110-μm-square mesas that then had contacts deposited and were rapid-thermal annealed (RTA) at 350°C for 30s. The first set of test structures (which will be called the VCSEL test set) was composed of the same material as the 980nm VCSELs but was etched into stripes rather than mesas to ease TEM sample preparation; the VCSEL test set did not receive contacts or an RTA cycle. The second set of test structures (which will be called the composition test set) consisted of three pairs of 100nm GaAs / 100nm $Al_xGa_{1-x}As$ layers for x=1.0 to 0.80 in x=0.02 steps, giving a total of 33 pairs. The composition was not graded at the GaAs / $Al_xGa_{1-x}As$ interfaces. This sample set was etched into stripes and did not receive contacts or an RTA cycle. The working VCSELs were oxidized at 450°C for 40 minutes in a tube furnace in flowing N_2 bubbled through 80°C H_2O. The test structures were oxidized at three separate temperatures. The oxidation temperatures and times were 440°C for 20min, 400°C for 150min and 360°C for 900min. The oxidation times were chosen so that the oxidation depth would be similar for each run. The flow of reactants was kept high enough to prevent any reactant-limited effects.

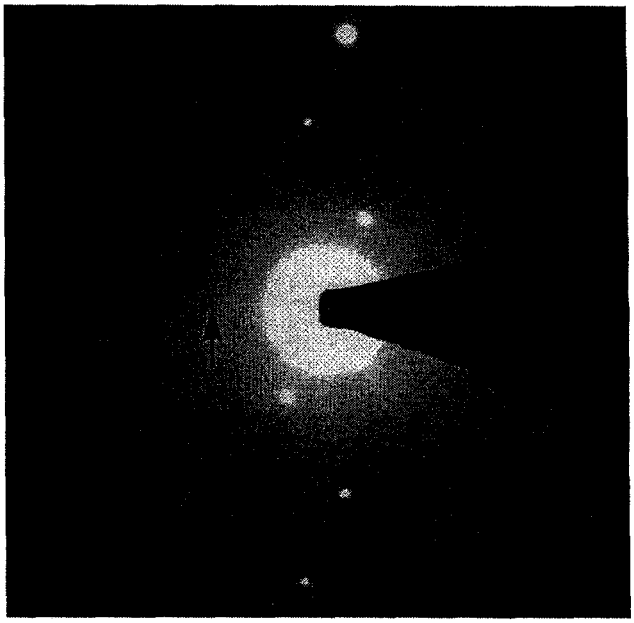

Figure 1: EDP of AlAs oxidized at 400°C. Three broad rings at corresponding to d-spacings of 1.41Å, 2.05Å and 2.4-3.3Å are indicated by the arrows. This EDP is typical of amorphous Al_2O_3. The sharp spots seen in the figure are from the surrounding GaAs.

The TEM samples were prepared by a combination of mechanical polishing and Ar-ion milling. As the oxide layers tended to be very susceptible to delamination, care was taken to keep the layers in compression during mechanical polishing. Water was used as a lubricant during all polishing steps, and mounting waxes were removed using ketones and alcohols. Images were formed using 200keV electrons for general imaging and as low as 20keV electrons for beam-induced crystallization studies. Care was taken to minimize thermal exposure, but the samples were heated to 100°C for ~60min in order to cure mounting epoxy and heated several times to ~80°C for a few seconds to mount the samples in wax for polishing.

3. OXIDE PHASE

Figure 1 shows an electron diffraction pattern (EDP) taken from an oxidized AlAs layer of the composition test set, which also contains the surrounding unoxidized GaAs layers. The diffraction pattern shows broad rings; the two most prominent correspond to d-spacings of 1.41Å, 2.05Å, with a third broad ring at 2.4~3.3Å. These diffuse rings indicate the oxide is in an amorphous rather than crystalline phase. This is supported by Figure 2 which shows a bright field image of an oxidized layer. The image reveals only granular, amorphous contrast and no hint of crystallites. The resolution of this image was aperture limited to 7Å. The diffraction patterns from layers of oxi-

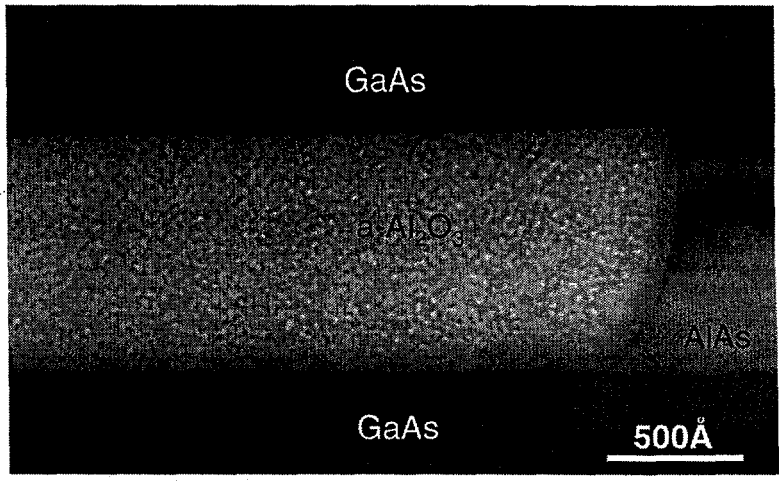

Figure 2: Bright-field image of oxidized AlAs near the oxide terminus. The oxide shows only granular, amorphous contrast. Note the change in the amorphous contrast in the oxide near the AlAs and lower GaAs interfaces. The crystalline AlAs and GaAs show some strain contrast but no extended defects have been observed. Also note the rounded shape of the oxide terminus.

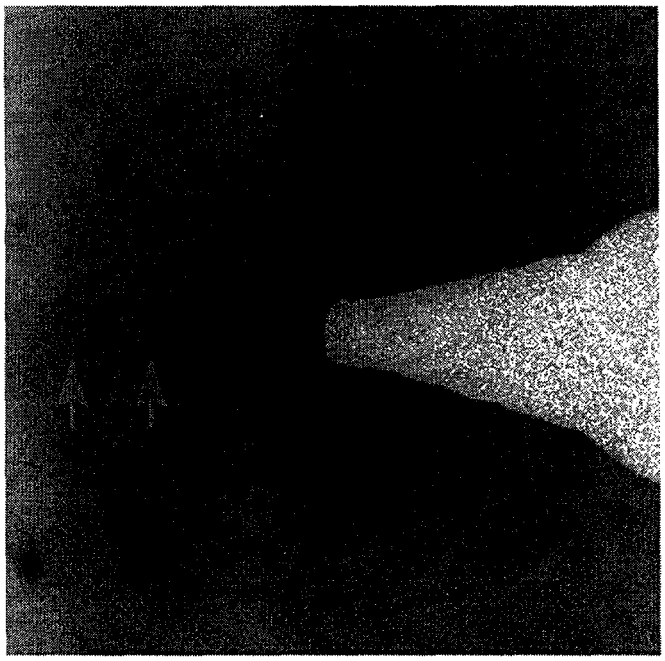

Figure 3: EDP of oxidized $Al_xGa_{1-x}As$, x=0.98, from a working VCSEL device that received an RTA treatment. The ring at d=1.41Å has sharpened considerably, and careful analysis of the ring at d=2.05Å indicates it has sharpened also. The broad ring near the origin is largely absent. The rings that have sharpened are those that are the strongest in the γ-Al_2O_3 EDP. The sharp spots are due to the surrounding GaAs layers, and the EDP is shown in negative contrast to assist the viewer.

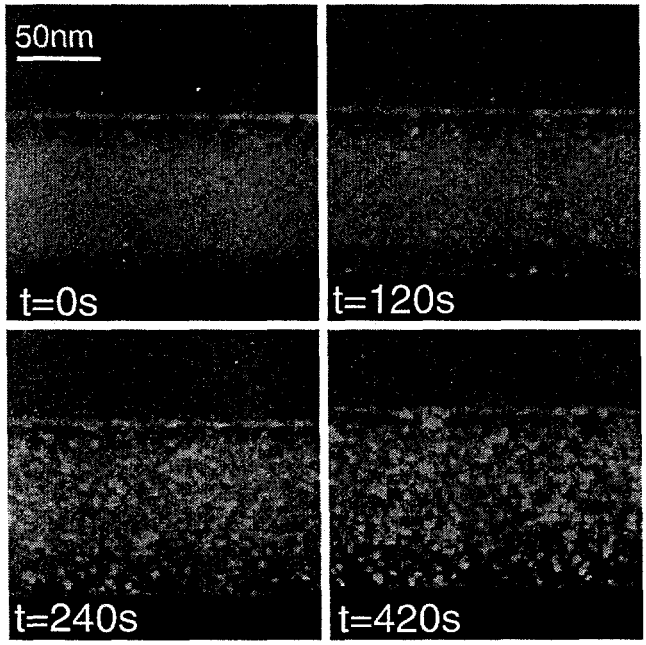

Figure 4: Dark-field images of oxidized $Al_xGa_{1-x}As$, x=0.98, from a working VCSEL device. The layer transformed from amorphous alumina to fine grained γ-Al_2O_3. The objective aperture contained part of the d=1.4Å ring and was not moved throughout the series. Intermediate images were recorded at 15s intervals.

dized $Al_xGa_{1-x}As$ (x=0.80 to 1.00) showed similar results.

Figure 3 shows an EDP from an oxidized $Al_{0.98}Ga_{0.02}As$ layer in a working VCSEL sample. This diffraction pattern is similar to Figure 1, but careful analysis indicates the rings at 1.4Å and 2.05Å have sharpened, while the broad ring close to the origin of the pattern is no longer present. This diffraction pattern was recorded under low-dose imaging conditions. While the change in the diffraction is subtle, we believe the change indicates that some crystalline phase is present in these materials even under low e-beam dose conditions. This phase is most likely γ-Al_2O_3 since the rings correspond to the strongest γ-Al_2O_3 rings and γ-Al_2O_3 has been identified in well crystallized material[9,10]. However, dark-field imaging of the crystalline phase was hampered by the unstable nature of the oxidized layer (see below).

Figure 4 shows a time sequence of dark-field images of an oxidized AlAs layer from sample set three. The position of the dark-field aperture was set on the 1.4Å ring and excluded the GaAs reflections. The electron beam was spread to approximately 1μm in diameter and was not adjusted through the course of the time sequence; however, the exact beam dose was not calibrated. The aperture limited, amorphous contrast initially seen transforms into a dense field of small crystallites. These crystallites are randomly oriented and ~5nm in diameter in the final image. Diffraction analysis of the final structure shows a series of sharp rings that indicate the grains are the cubic gamma phase of Al_2O_3. This transformation does not depend on the fraction of Al in the oxidized layer, but detailed transformation rates were not measured.

The cause of the phase transformation was investigated. Direct electron, knock-on damage was ruled out by using low electron energies. Figure 5 shows two EDPs recorded using 40keV electrons. Figure 5a was recorded using low-dose techniques while Figure 5b was recorded after a 60s exposure to 40keV electrons. The sharp rings present in Figure 5b indicate the crystalline transformation has begun. Similar results were also observed at 20keV. The maximum energy transferred to an atom by an electron is small due to the small electron mass. For 20keV electrons, the maximum energy transfer is 1.5eV for Al, 2.6eV for O, and 41eV for H. The knock-on energy is of an order of magnitude too small to displace Al or O[11], but it may be sufficient to displace H and could indicate a hydroxide-to-oxide phase transition. However, the amount of H in the layer is too small for the oxidized material to be a hydroxide phase (see below). Local, e-beam-induced

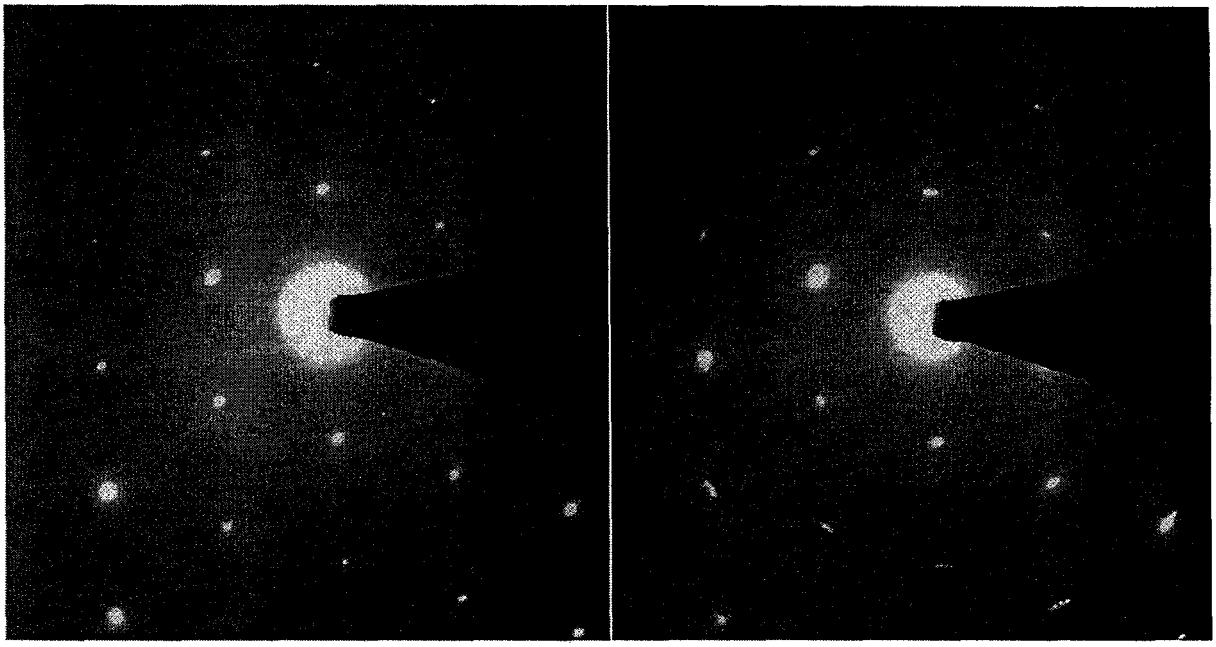

Figure 5: EDP recorded using 40keV electrons both before a) and after b) 60s high intensity electron beam exposure of an oxidized $Al_xGa_{1-x}As$ x=0.92 layer. Before exposure, only amorphous rings are seen while after exposure, polycrystalline γ-Al_2O_3 is observed. The sharp spots in both EDPs are from the surrounding GaAs layers.

heating is also an unlikely cause of the crystallization, since the crystallization is seen at the electron beam position and does not show evidence of thermal diffusion.

It is likely that the local crystallization observed is the result of electron-induced ionization processes. These processes require very little energy transfer and typically result in enhanced mobility of the ionized atom[12]. This could cause local transformation of the structure to the crystalline gamma phase.

4. OXIDE COMPOSITION

Figure 6 shows portions of energy-dispersive x-ray spectra (EDXS) generated using 200keV electrons from oxidized and unoxidized $Al_{0.92}Ga_{0.08}As$ layers. Upon oxidation, the Ga signal is unchanged, but the As signal is greatly reduced. It is assumed that the Ga remains in the layer as the solid solution $(Al_xGa_{1-x})_2O_3$, since no elemental Ga precipitates were observed and crystallized γ-Ga_2O_3 is distinguishable from γ-$(Al_{0.92}Ga_{0.08})_2O_3$ by the 3.7% change in lattice constant. The very low As signal is puzzling since As has been identified in oxidized layers by other authors[7,8]. It is possible that the As is lost via electron-beam-induced effects or excess H in the oxide layer[7]; this question is currently under investigation.

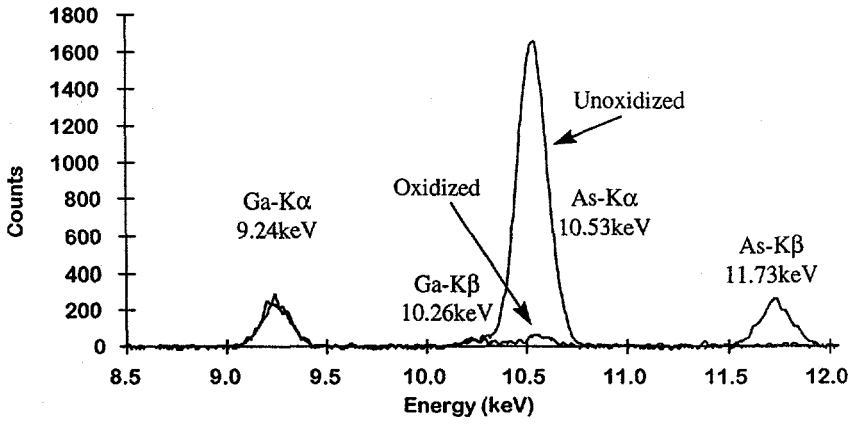

Figure 6: A portion of an EDXS spectrum from oxidized and unoxidized regions of an $Al_xGa_{1-x}As$ x=0.92 layer. The Ga and the Al (not shown) are retained in the layer upon oxidation, but the As is markedly reduced.

As mentioned above, hydrogen may play a role in stabilizing the amorphous material. There are several forms of $Al(OH)_3$ and AlOOH which are found as poorly crystallized minerals[6]. To distinguish between the formation of the hydroxide rather than the more stable oxide (Al_2O_3) phases, the hydrogen content was measured. Figure 7 shows the local H content of a film consisting of a 100nm GaAs cap and a 500nm AlAs layer oxidized at 400°C as measured using elastic recoil detection

(ERD) of atoms scattered from the film by 30MeV Si^{5+}. Assuming all of the Al originally in the AlAs layer is retained upon oxidation, the measured H density of ~$(1.1\pm0.1)x10^{21}cm^{-3}$ gives an Al-to-H ratio of 20:1, not the 1:1 or 1:3 ratios of the hydroxide phases.

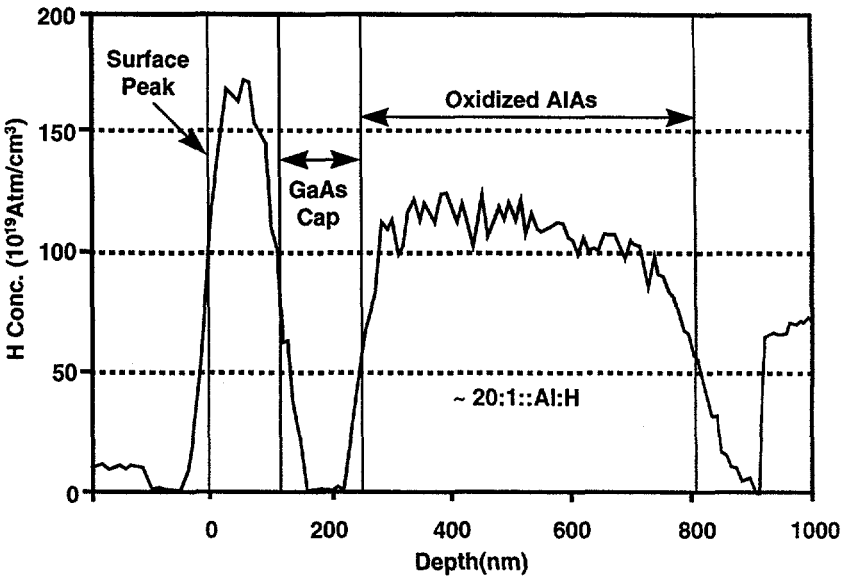

Figure 7: Hydrogen content of laterally oxidized AlAs measured using 30MeV Si^{+5} elastic recoil detection. Assuming the all the Al is retained in the layer after oxidation, the measured H content gives a 20:1 Al to H ratio. This is far too little H for the amorphous phase to be a hydroxide.

5. OXIDE / GaAs INTERFACE

The interface of the $(Al_xGa_{1-x})_2O_3$ with the unoxidized GaAs is abrupt, as seen in Figure 2. High resolution images (not shown) indicate a sharp transition from amorphous oxide to single crystal GaAs with no evidence for interfacial precipitates. Conventional images (Figure 2) show some strain at the interface that is likely due to the relaxation of the thin foil TEM sample.

Recent reports suggest the presence of voids[10] or inclusions[9] at the oxide/GaAs interface. Figure 8 shows a time sequence of the interfacial structure during e-beam-induced crystallization. The bright-field images reveal the crystallization process through the loss of the granular, amorphous contrast. Also present in the image are voids at the oxide/GaAs interface. This voiding is correlated with the loss of amorphous contrast in the images and is the result of a local contraction of the oxide layer upon crystallization.

Figure 9 shows images of oxidized layers near the edge of the etched mesa that admits the H_2O for lateral oxidation. There is a thin layer of polycrystalline material between the single crystal GaAs and the amorphous oxidized $Al_xGa_{1-x}As$ that thickens as the Al content of the oxidized layer increases. This material has been identified as cubic Ga_2O_3, which has a similar structure to γ-Al_2O_3 but a lattice constant of 8.22Å, compared to 7.9Å for Al_2O_3. This identification was obtained using EDXS and diffraction analysis (see Figure 10). The crystal grains are well formed and oriented with respect to the original GaAs layer, indicating the lack of an amorphous intermediate phase. The

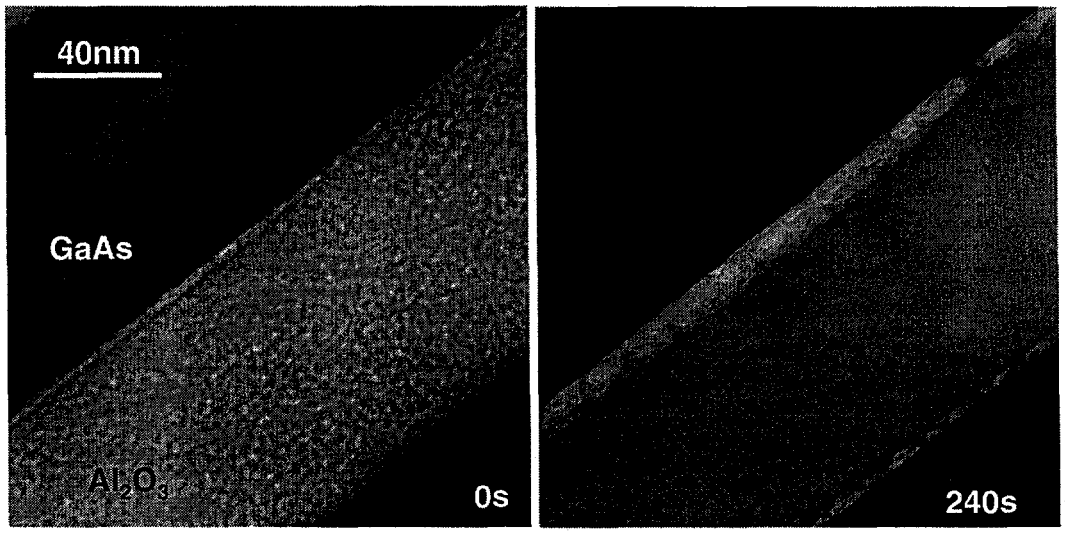

Figure 8: Interface voiding resulting from electron-beam-induced crystallization. Crystallization is evidenced by the loss of the granular contrast in the Al_2O_3 layer.

thickness of the Ga_2O_3 increases with increasing Al content of the adjoining oxidized layer. This relationship is explained as follows: Since the Al_2O_3 acts as a conduit for reactants to the unoxidized AlAs, it also brings reactants to the unoxidized GaAs adjoining the oxidized layer. Since the oxidation rate of $Al_xGa_{1-x}As$ increase with Al content, the time the GaAs is exposed to the oxidants will increase with the Al content of the adjoining layer for a given distance from the mesa edge. Thus the Ga_2O_3 layer next to the AlAs layer is thicker because it has been in contact with the oxidants longer than the Ga_2O_3 layer next to the $Al_{0.80}Ga_{0.20}As$ layer.

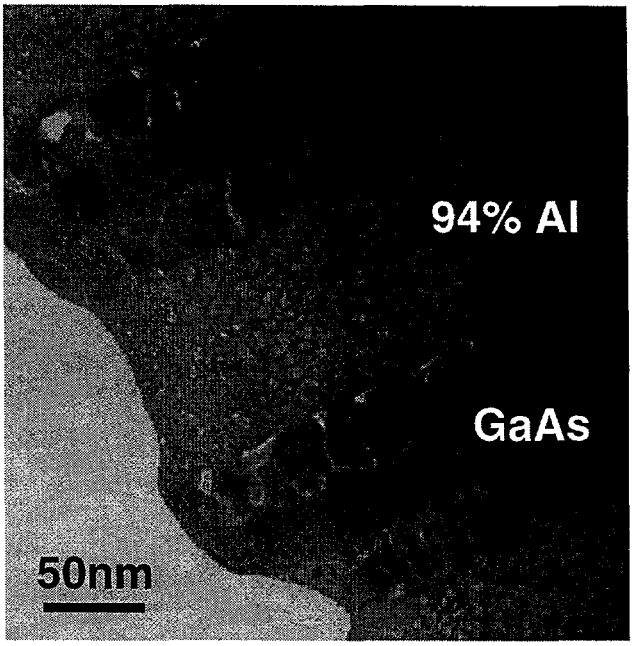

Figure 9: Cubic Ga_2O_3 grains are seen in the GaAs layers surrounding an oxidized $Al_xGa_{1-x}As$, x=0.94, layer near a mesa edge. The grains are only seen near the edge, and their thickness increases with increasing Al content of the surrounding oxidized layers.

6. OXIDE /AlGaAs INTERFACE

Images of the structure show very little strain contrast around the oxide terminus (Figure 2), and low-magnification, cross-sectional images of the structure have not revealed extended defects emanating from the oxide layers[5,9]. This is consistent with the excellent performance and stability of these structures[2,3,4].

The shape of the oxide terminus can affect the VCSEL performance by modifying the gain of the optical modes[13]. Figure 11 shows the oxide fronts of a working VCSEL, while Figure 2 is that of a test structure. The shape of the oxide front in the VCSEL set is rounded, which is expected since the layer was intentionally graded from pure GaAs to $Al_xGa_{1-x}As$; this causes the edges of the oxide front to react more slowly than the center. However, the test structure was grown with abrupt interfaces and still shows a tilted oxide front with rounded edges at the interface. This slightly nonuniform oxidation rate is likely due to variations in strain near the oxide terminus as the reaction front is propagating into the $Al_xGa_{1-x}As$.

Another feature of the oxide / $Al_xGa_{1-x}As$ interface is an ~17nm interface zone that is seen in both Figure 2 and Figure 11. This zone shows a different amorphous contrast than the remainder of the oxide and does not crystallize under the electron beam. We are presently investigating the composition of this zone.

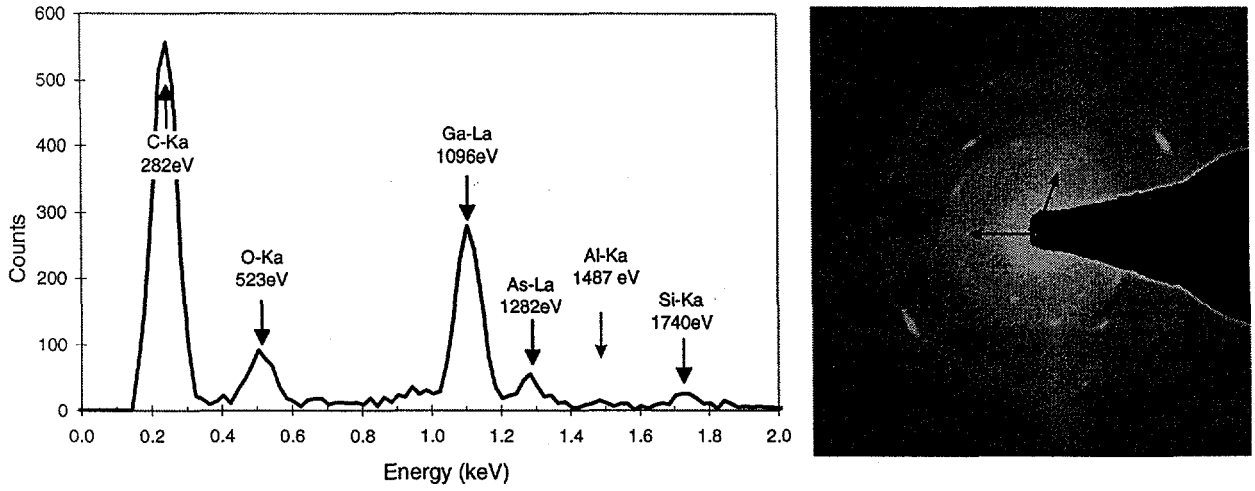

Figure 10: Characterization of Ga_2O_3. The EDXS spectrum (right) shows clear Ga and O peaks with very little As and Al. The C peak is due to contamination and the Si peak is due to redeposition during ion-beam milling. The EDP (left) shows a spotty set of rings that can be index to γ-Ga_2O_3 with a lattice constant of 8.22Å. The pattern is aligned to the surrounding GaAs crystal, whose (111) reflections are shown by the black arrows. The adjacent, amorphous Al_2O_3 gives the broad rings seen in the pattern.

7. CONCLUSION

Not only has lateral oxidation of $Al_xGa_{1-x}As$ proven to be useful from a optoelectronic standpoint, but it is also a complex material system. We have shown that lateral oxidation produces an amorphous phase of $(Al_xGa_{1-x})_2O_3$ that is unstable under the electron beam of the TEM where it transforms to γ-$(Al_xGa_{1-x})_2O_3$. The GaAs interfaces are abrupt but the GaAs can oxidize through the $(Al_xGa_{1-x})_2O_3$. The interface with the unoxidized $Al_xGa_{1-x}As$ shows an amorphous transition region that is stable under the electron beam and has a different amorphous character than the remainder of the $(Al_xGa_{1-x})_2O_3$. The amount of As in the oxidized layers is drastically reduced. This reduction may be related to the high background hydrogen ($1.1x10^{21}cm^{-3}$) in the oxide.

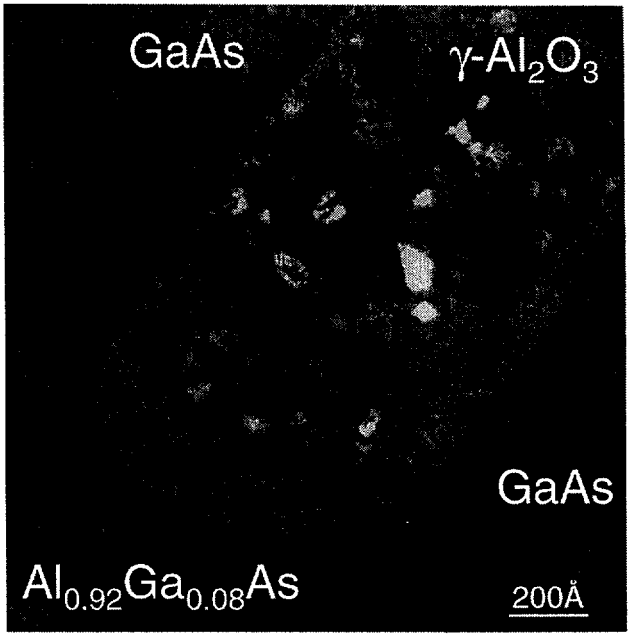

Figure 11: The oxidation front in a working VCSEL device. The dark-field image shows both the fine-grained γ-$(Al_xGa_{1-x})_2O_3$ and the amorphous interface zone. Note the oxidation front is not flat but curved and the amorphous zone tapers back away from the oxide front. Compare to Figure 2.

ACKNOWLEDGMENTS

The authors wish to thank M.P. Moran, K.M. Geib and H.Q. Hou for invaluable technical assistance, C.I.H. Ashby, O. Blum, R. Hull, and D.T. Mathes for many useful discussions, D.S. Walsh and B.L. Doyle for ERD analysis, and J.C. Barbour for access to unpublished data. This work was supported by the U.S. Department of Energy under contract DE-AC04-94AL85000. Sandia is a multiprogram laboratory operated by Sandia Corporation, a Lockheed Martin Company, for the U.S. Department of Energy.

REFERENCES

[1] J. M. Dallessasse, N. Holonyak, Jr., A. R. Sugg, T.A. Richard and N. El-Zein, "Hydrolyzation oxidation of $Al_xGa_{1-x}As$-AlAs-GaAs quantum-well heterostructures and superlattices", Appl. Phys. Lett. **57**, 2844 (1990).

[2] D.L. Huffaker, D.G. Deppe, K. Kumar, and T.J. Rogers, "Native-oxide defined ring contact for low-threshold vertical-cavity lasers", Appl. Phys. Lett. **65**, 97 (1994).

[3] K. D. Choquette, R. P. Schneider, Jr., K. L. Lear, and K. M. Geib, "Low-threshold voltage vertical-cavity lasers fabricated by selective oxidation", Electron Lett. **30**, 2043 (1994).

[4] G.M. Yang, M.H. MacDougal, P.D. Dapkus, "Ultralow threshold current vertical-cavity surface-emitting lasers obtained with selective oxidation", Electron Lett. **31**, 886 (1995).

[5] K. D. Choquette, K. L. Lear, R. P. Schneider, Jr., K. M. Geib, J. J. Figiel, and R. Hull, "Fabrication and performance of selectively oxidized vertical-cavity lasers", IEEE Photonics Technol. Lett. **7**, 1237 (1995).

[6] B.C. Lippens and J.J. Steggerda "Active alumina", *Physical and Chemical Aspects of Adsorbents and Catalysts*, edited by B.G. Linsen p.171-213 (Academic Press, London, 1970).

[7] C.I.H. Ashby, J.P. Sullivan, K. D. Choquette, K. M. Geib, H.Q. Hou, "Wet oxidation of AlGaAs: the role of hydrogen", Appl. Phys. Lett. To Appear.

[8] Z. Liliental-Weber, Private Communication.

[9] R.D. Twesten, D.M. Follstaedt, K. D. Choquette, and R. P. Schneider, Jr., "Microstructure of laterally oxidized $Al_xGa_{1-x}As$ layers in vertical-cavity lasers", Appl. Phys. Lett. **69**, 19 (1996).

[10] S. Guha, F. Agahi, B. Pezeshki, J.A. Kash, D.W. Kisker and N.A. Bojarczuk, "Microstructure of AlGaAs -oxide heterolayers formed by wet oxidation", Appl. Phys. Lett. **68**, 906 (1996).

[11] L.W. Hobbs, "Radiation damage in electron microscopy of inorganic solids", Ultramicroscopy, **3**, 381 (1979).

[12] L. Reimer, *Transmission Electron Microscopy 2ND Ed.*, p453-457 (Springer-Verlag, Berlin, 1989).

[13] E.R. Hegblom, D.I. Babic, B.J. Thibeault, L.A. Coldren, "Estimation of scattering losses in dielectrically apertured vertical-cavity lasers" Appl. Phys. Lett., **68**,1757 (1996).